Proximity-dependent biotinylation and identification of flagellar proteins in *Trypanosoma cruzi*

Madalyn M. Won[1], Aaron Baublis[2], Barbara A. Burleigh[1]

[1]Department of Immunology and Infectious Diseases, Harvard T. H. Chan School of Public Health Boston, MA 02115, USA

[2]Harvard Chan Advanced Multi-omics Platform, Harvard T.H. Chan School of Public Health, Boston, Massachusetts 02115, USA

Corresponding Author: Barbara Burleigh: bburleig@hsph.harvard.edu

Running Title: Flagellar protein identification in *Trypanosoma cruzi*

Abstract

The flagellated kinetoplastid protozoan and causative agent of human Chagas disease, *Trypanosoma cruzi,* inhabits both invertebrate and mammalian hosts over the course of its complex life cycle. In these disparate environments, *T. cruzi* uses its single flagellum to propel motile life stages and in some instances, to establish intimate contact with the host. Beyond its role in motility, the functional capabilities of the *T. cruzi* flagellum have not been defined. Moreover, the lack of proteomic information for this organelle, in any parasite life stage, has limited functional investigation. In this study, we employed a proximity-dependent biotinylation approach based on the differential targeting of the biotin ligase, TurboID, to the flagellum or cytosol in replicative stages of *T. cruzi,* to identify flagellar-enriched proteins by mass spectrometry. Proteomic analysis of the resulting biotinylated protein fractions yielded 218 candidate flagellar proteins in *T. cruzi* epimastigotes (insect stage) and 99 proteins in intracellular amastigotes (mammalian stage). Forty of these flagellar-enriched proteins were common to both parasite life stages and included orthologs of known flagellar proteins in other trypanosomatid species, proteins specific to the *T. cruzi* lineage and hypothetical proteins. With the validation of flagellar localization for several of the identified candidates, our results demonstrate that TurboID-based proximity proteomics is an effective tool for probing subcellular compartments in *T. cruzi.* The proteomic datasets generated in this work offer a valuable resource to facilitate functional investigation of the understudied *T. cruzi* flagellum.

Importance

Trypanosoma cruzi is a protozoan parasite that causes Chagas disease, which contributes substantial morbidity and mortality in South and Central America. Throughout its life cycle, *T. cruzi* interacts with insect and mammalian hosts via its single flagellum, establishing intimate contact with host membranes. Currently, few flagellar proteins have been identified in *T. cruzi* that could provide insight into the mechanisms involved in mediating physical and biochemical interactions with the host. Here, we set out to identify flagellar proteins in the main replicative stages of *T. cruzi* using a proximity-labeling approach coupled with mass spectrometry. The >200 candidate flagellar proteins identified represent the first large scale identification of candidate flagellar proteins in *T. cruzi* with preliminary validation. These data offer new avenues to investigate the biology of *T. cruzi* - host interactions, a promising area for development of new strategies aimed at the control of this pathogen.

Introduction

Trypanosoma cruzi is the uniflagellate protozoan parasite that causes Chagas disease, a chronic disease with severe outcomes including cardiomyopathies and gastrointestinal motility disorders [1,2]. *T. cruzi* has a complex life cycle that involves both invertebrate and mammalian hosts, in which the parasite undergoes marked developmental changes and alternates between actively dividing ('epimastigote' or 'amastigote' forms in insect and mammalian hosts, respectively) and non-dividing 'trypomastigote' forms in both hosts (life cycle schematic; **Supplementary Fig. 1**). In mammals, infection is initiated by motile trypomastigotes that actively invade host cells before converting to the non-motile amastigote stage that replicates in the host

62 cytoplasm. Intracellular *T. cruzi* amastigotes begin to replicate ~24 hours post-infection
63 (hpi) and undergo several rounds of cell division before converting back to
64 trypomastigotes that eventually rupture the host cell membrane (between ~90-120 hpi)
65 to allow dissemination of the parasite and infection of new tissue sites. Once *T. cruzi*
66 infection is established in mammalian hosts, parasites typically persist at low levels for
67 the life of the host, giving rise to chronic infections that can trigger inflammation and
68 pathology.

69 In both insect and mammalian hosts, *T. cruzi* can establish intimate contact with
70 host structures using its single flagellum [3–5]. In triatomine vectors, epimastigotes attach
71 to the hindgut by forming a hemidesmosome-like structure between the distal part of the
72 flagellum and host rectal epithelium [5]. This attachment prevents the parasites from
73 being flushed from the insect and is important for promoting differentiation to the
74 infectious metacyclic stage [5]. In mammalian host cells, cytosolically-localized *T. cruzi*
75 amastigotes establish intermittent contact with host mitochondria using their short motile
76 flagellum [3,6]. Unlike the motile trypomastigote and epimastigote stages of *T. cruzi,* that
77 have elongated flagella (up to 15 μm in length [7]), replicative intracellular amastigotes
78 have a truncated flagellum (~2.7 μm) that extends just beyond the opening of the
79 flagellar pocket [6]. Also, *T. cruzi* amastigotes retain a 9+2 axonemal structure found in
80 motile trypanosomatid life stages [8], but lack a paraflagellar rod, a unique lattice-like
81 structure that runs parallel to the axoneme in these organisms [9], and which is
82 associated with several functions including flagellar motility and signal transduction [10]. It
83 has long been assumed that the minimal amastigote flagellum serves no function other
84 than to provide a structural platform for flagellar outgrowth during differentiation to

85 motile life stages [11]. However, recent observations that the flagellum of intracellular *T.*
86 *cruzi* amastigotes undergoes low frequency aperiodic 'beating' inside mammalian host
87 cells [6] and makes physical contact with the host mitochondria [3,6], indicate that the
88 amastigote flagellum has a functional role within the host cell. The interaction between
89 the *T. cruzi* amastigote flagellum and host mitochondria is comparable to the intimate
90 contact observed between the flagellum of intracellular *Leishmania mexicana*
91 amastigotes and the host parasitophorous vacuole membrane [12]. In the case of
92 *Leishmania*, it has been postulated that the amastigote flagellum has a sensory role
93 and/or functions in the delivery of parasite material to the infected host cell [12,13]. It is
94 therefore reasonable to predict that the *T. cruzi* amastigote flagellum may have similar
95 role(s) in its interactions with the intracellular environment of the host cell.

96 In addition to critical roles in motility, eukaryotic flagella (i.e. cilia) and non-motile
97 cilia have emerged as important sensory organelles that are equipped with signal
98 transduction systems and second messengers such as cyclic AMP (cAMP) [14] and
99 calcium [15,16] that coordinate cellular responses to external stimuli. Functions beyond cell
100 locomotion have also been ascribed to the flagellum of motile trypanosomatid life stages
101 [11,13,17–19], where the best understood example of sensory integration in these organisms
102 is the role of flagellar receptor-type adenylate cyclases and cAMP-depending signaling
103 in pH taxis and social motility in the insect stage of *Trypanosoma brucei* [20–23]. In
104 *Leishmania*, flagellar aquaporin has been implicated in osmotaxis [24] in the insect stage,
105 and the flagellar membrane may be a critical site for glucose [25,26] and arginine [27]
106 sensing in these parasites. Indeed, in both *T. brucei* and *Leishmania*, near
107 comprehensive flagellar proteomes have been generated using shot-gun proteomics of

108 isolated flagella [28–30] or of detergent and high salt extracted fractions of the parasite,
109 yielding axonemal and paraflagellar rod proteins [31]. Further, in *T. brucei*, specific
110 domains of the flagellum have been partially mapped using proximity-dependent
111 biotinylation including flagellar attachment zone proteins [32] and the flagellar tip [33], a
112 specialized signaling domain.

113 By comparison, we have little knowledge of the molecular composition of the *T.*
114 *cruzi* flagellum. Beyond a core axonemal proteome that is predicted based on
115 conservation across trypanosomatid species and life stages [34], few flagellar proteins
116 that have the potential to serve as a functional interface with the host environment have
117 been identified in any *T. cruzi* life stage [9,35,36]. The best characterized is the flagellar
118 calcium-binding protein (FCaBP), a dual-acylated, 24 kDa Ca^{2+}-sensing protein that
119 tethers to the inner leaflet of the flagellar membrane [37]. FCaBP is expressed in all *T.*
120 *cruzi* life stages and is conserved across other trypanosomatid species, but its precise
121 role in the biology of these organisms is unknown beyond its role as a calcium binding
122 protein [36,38,39]. Additionally, we have recently localized small myristoylated protein 1-1
123 (TcSMP1-1) to the flagellum in amastigotes [6], but the overall proteomic landscape of the
124 *T. cruzi* flagellum remains largely uncharacterized.

125 In this study, we pursued a targeted, proximity-dependent biotinylation (BioID)
126 approach to identify flagellar membrane and membrane-proximal flagellar proteins in
127 the replicative stages of *T. cruzi.* We report the identification of 218 and 99 candidate
128 flagellar proteins in *T. cruzi* epimastigotes and intracellular amastigote stages,
129 respectively, many of which are conserved in other trypanosomatid species with
130 evidence of flagellar localization. Approximately 20% of the candidate flagellar proteins

131 were found to be restricted to the *T. cruzi* lineage, including a hypothetical protein that
132 we confirmed localizes to the flagellar tip in *T. cruzi* epimastigotes and intracellular
133 amastigotes. The novel BioID dataset identified here provides a critical foundation for
134 investigation of the *T. cruzi* flagellum and its role in mediating interactions with diverse
135 host environments.
136

137 **Results**

138 **Flagellar and cytosolically targeted TurboID retains activity in *T. cruzi***

139 To facilitate the identification of flagellar proteins in *T. cruzi* using a proximity-
140 dependent biotinylation approach, we generated transgenic parasites that express the
141 biotin ligase, TurboID [40] in the parasite flagellum, as an in-frame fusion with C-terminal
142 FLAG-tagged *T. cruzi* small myristoylated protein 1-1 (TcSMP1-1) (**Fig. 1A,B;** SMP1-1-
143 FLAG-TurboID; **'***F-Turbo'*). TcSMP1-1 was chosen as the endogenous 'bait' protein for
144 flagellar localization of TurboID given its near exclusive localization in the flagellum in
145 both replicative stages of *T. cruzi*, epimastigotes and amastigotes [6] (**Fig. 1A**), and
146 because TcSMP1-1 contains the N-myristoylation sequence motif (MGXXXS/T)
147 required for localization and tethering to the inner flagellar membrane, as demonstrated
148 in *Leishmania* [41]. The strategy of targeting TurboID to the flagellum using TcSMP1-1 is
149 expected to increase the likelihood of identifying flagellar membrane and associated
150 proteins while minimizing capture of axonemal proteins. To control for non-flagellar
151 TurboID expression in the F-Turbo parasites, we generated an independent transgenic
152 line that expresses FLAG-TurboID in the cytoplasm (**Fig. 1B; '***C-Turbo'*). The parallel
153 processing of F-Turbo and C-Turbo parasites, along with parental (WT) parasites that

154 lack TurboID expression (**Fig. 1C)**, will allow for background subtraction and
155 identification of flagellar-enriched proteins in F-Turbo versus C-Turbo within the same
156 parasite life cycle stage.

157 TurboID expression in transgenic *T. cruzi* parasites was confirmed by indirect
158 immunofluorescence microscopy of fixed parasites stained with an antibody to the
159 FLAG tag epitope, located immediately upstream of TurboID (**Fig. 2**). The flagella of F-
160 Turbo parasites were brightly stained (**Fig. 2A,C;** *F-Turbo*) indicating that trafficking of
161 TurboID to the flagellum occurred in both *T. cruzi* epimastigote (**Fig. 2A;** *F-Turbo*) and
162 amastigote (**Fig. 2C;** *F-Turbo*) life stages. While most of the FLAG signal was localized
163 to the flagellum in epimastigotes (**Fig. 2A;** *F-Turbo*), signal was detected in the body of
164 intracellular amastigotes in addition to the brightly stained flagellum (**Fig. 2C;** *F-Turbo*),
165 which may be due to overexpression of the SMP1-1-FLAG-TurboID fusion protein. C-
166 Turbo parasites, generated as a proteomic control for non-flagellar TurboID-dependent
167 biotinylation (**Fig. 1C**), were confirmed to express cytosolic FLAG in both parasite life
168 stages (**Fig. 2A,C;** *C-Turbo***)**. To determine if TurboID is active in *T. cruzi*, total protein
169 lysates were prepared from WT and Turbo-expressing parasites, following brief
170 exposure to exogenous biotin, were probed with streptavidin-DyLight™ 800 to detect
171 biotinylated proteins (**Fig. 2B,D**). As expected, multiple biotinylated proteins were
172 revealed in lysates derived from F-TurboID and C-TurboID epimastigotes (**Fig. 2B**) and
173 amastigotes (**Fig. 2D**) whereas few biotinylated proteins were detected in the parental
174 (WT) controls. Differences in the biotinylated protein profiles observed when comparing
175 F-Turbo to C-Turbo within a single life stage (**Fig. 2B,D)** likely reflect the differential
176 localization patterns for TurboID in these parasite lines. Combined, these results

177 confirm the expression of active TurboID in the flagellum (F-Turbo) or cytosol (C-Turbo)
178 in both replicative stages of *T. cruzi*.
179
180 **Proteomic identification of candidate flagellar proteins in *T. cruzi***
181 Biotinylated proteins in lysates generated from WT, F-Turbo and C-Turbo *T. cruzi*
182 epimastigotes or intracellular amastigotes, were captured on immobilized streptavidin
183 beads and identified using high performance liquid chromatography combined with
184 mass spectrometry (**Fig. 1C**). Three independent biological replicates were analyzed for
185 each parasite line, with the exception of F-Turbo epimastigotes, for which triplicate
186 samples from two independent transfections were included. Peptide identification and
187 relative intensity data obtained for replicate samples from each parasite line are
188 represented in **Supplementary Table 1**. Principal component analysis (PCA) identified
189 overall trends in the proteomic data obtained for *T. cruzi* epimastigotes (**Fig. 3A**) and
190 amastigotes (**Fig. 3C**), revealing that biological replicates from individual parasite lines
191 (WT, F-Turbo, C-Turbo) formed discrete clusters that were well separated from each
192 other. As the replicates from independent F-Turbo epimastigote lineages were
193 indistinguishable, these samples were pooled for subsequent analyses. Prior to data
194 filtering and analysis, protein intensity scores were averaged across biological replicates
195 within individual experimental groups (**Supplementary Table 1**).
196 Streptavidin-bound proteins identified by mass spectrometry in WT parasites
197 (which lack TurboID) represent the 'background' signal of endogenously biotinylated
198 proteins and proteins that bound non-specifically to immobilized streptavidin. Thus,
199 proteins represented at less than 100-fold enriched over the WT samples in F-Turbo or

200 C-Turbo epimastigote samples were removed before subsequent analysis. Also, any
201 proteins identified in less than 4/6 of the F-Turbo samples were removed
202 (**Supplementary Table 2**). Volcano plots revealed the protein subsets significantly
203 enriched in F-Turbo and C-Turbo samples in epimastigotes (**Fig. 3B**) and amastigotes
204 (**Fig. 3D**). Proteins found to be significantly enriched in F-Turbo over C-Turbo (fold-
205 change > 2; q-value ≤ 0.01) as well as proteins identified uniquely in F-Turbo samples
206 (i.e., not present in C-Turbo samples from the same parasite life stage) are listed in
207 **Supplementary Table 3**. From this analysis, 218 proteins were identified as
208 significantly enriched in F-Turbo samples from *T. cruzi* epimastigotes and 99 proteins in
209 amastigotes (**Supplementary Table 3**).
210
211 **The *T. cruzi* SMP1-1 proximity proteome includes known trypanosomatid flagellar**
212 **proteins.**
213 The searchable TrypTag database [42], which contains localization data for 7,487
214 *T. brucei* proteins, was used as a resource to identify orthologues in the *T. cruzi*
215 flagellar-enriched protein dataset (**Supplementary Table 3**) that have demonstrated
216 flagellar localization in *T. brucei*. Of the 218 flagellar-enriched proteins in *T. cruzi*
217 epimastigotes, 145 have orthologs that are represented in the TrypTag database and of
218 these, 75 proteins exhibit at least partial flagellar localization in *T. brucei* bloodstream
219 forms [42]. Similar results emerged from the *T. cruzi* amastigote data where orthologs of
220 75 of the 99 proteins found to be enriched in amastigote F-Turbo samples had orthologs
221 in *T. brucei* and were endogenously tagged, 44 of these showed at least partial flagellar
222 localization. A comparison of the flagellar-enriched proteins identified in both *T. cruzi*

223 epimastigotes and amastigotes revealed 40 proteins common to both life stages (**Fig.**
224 **3E**), of which 29 have orthologs that are represented in the TrypTag database
225 (**Supplementary Table 3**) and 20 proteins exhibited some flagellar localization in *T.*
226 *brucei*. Examples of confirmed flagellar proteins in other trypanosomatids that are
227 significantly enriched in the *T. cruzi* flagellar proximity proteome include: flagellar
228 membrane 8 [43], flabarin [44], flagellar attachment zone 14 [32], casein kinase I [42], CARP3 [20]
229 and cysteine peptidase, Clan CA, family C2 (calpain 1.3) [42]. Although a significant
230 proportion of the flagellar candidates identified in *T. cruzi* epimastigotes and
231 amastigotes fall into the 'hypothetical' category (i.e., no annotation), the datasets were
232 found to be enriched in kinase domains, calpain domains, and small GTP binding
233 protein / GTPase domains (**Fig. 3F**).
234

235 **Selected flagellar candidates localize to the *T. cruzi* flagellum in epimastigotes**
236 **and amastigotes.**

237 To localize candidate flagellar proteins in *T. cruzi*, we prioritized those that were
238 significantly enriched in both the epimastigote and amastigote F-Turbo datasets and
239 that included one or more of the following characteristics: (a) sequence motifs predicting
240 membrane localization; (b) predicted role in signaling based on annotation or (c) were
241 unique to the *T. cruzi* lineage (i.e., no obvious orthologues in other trypanosomatid
242 species). Based on these criteria, six proteins were selected for endogenous FLAG-
243 tagging and subsequent subcellular localization (**Table 1**) using primers and homology-
244 directed repair templates shown in (**Supplementary Fig. 4**). Four of the 6 proteins were
245 successfully tagged and three of which exhibited flagellar localization in *T. cruzi*

246 epimastigotes: calpain 1.3 (TcCLB.506563.200), CARP3 (TcCLB.506681.40) and
247 hypothetical protein (TcCLB.510329.180) (**Fig. 4A; Supplementary Fig. 2)**. Another
248 hypothetical protein (TcCLB.509965.20) was not verified as flagellar as the FLAG
249 epitope signal localized to the parasite body (data not shown). Calpain 1.3-mRuby2-
250 smFP FLAG exhibited a punctate pattern of labeling along the entire length of the *T.*
251 *cruzi* epimastigote flagellum (**Fig. 4A**), whereas expression appeared to be restricted to
252 the flagellar tip in the intracellular amastigote stage (**Fig. 4B**). Both CARP3 and the
253 hypothetical protein (TcCLB.510329.180) localized to the distal region of the
254 epimastigote flagellum (**Fig. 4A**) and hypothetical protein (TcCLB.510329.180) also
255 localized to the flagellar tip in amastigotes (**Fig. 4B**). We were unable to determine
256 CARP3 localization in amastigotes, due to undetectable signal for CARP3-mRuby2-
257 smFP FLAG expression in this life stage, despite clear signal and flagellar localization in
258 epimastigotes (**Fig. 4A**). Nonetheless, the successful identification of a subset of
259 flagellar-localized proteins in intracellular *T. cruzi* amastigotes and epimastigotes
260 provides initial validation of the proteomic datasets generated from proximity-dependent
261 labeling.
262

263 **Discussion**

264 In the present work we demonstrate the successful use of a proximity labeling
265 tool in the protozoan parasite, *Trypanosoma cruzi.* With the goal of identifying flagellar
266 membrane and/or associated proteins in *T. cruzi* as candidates for mediating physical or
267 functional interactions with insect or vertebrate hosts, the biotin ligase TurboID was
268 targeted to the parasite flagellum as a fusion protein with the inner flagellar membrane

269 protein, SMP1-1. Overexpression of the fusion protein was well-tolerated in the parasite,
270 with no interference in the ability to transition between axenic epimastigotes, the *T. cruzi*
271 life stage in which DNA transfection and selection is performed, and the intracellular
272 stages in mammalian cells. This offered the opportunity to perform a comparative
273 analysis of the two main replicative stages of *T. cruzi*, one that is motile with an
274 elongated flagellum (epimastigote) and the other that is non-motile with a short
275 flagellum (intracellular amastigote). Furthermore, inclusion of cytosolic-TurboID
276 expressing parasites in the analysis aided in the differential identification of flagellar-
277 enriched biotinylated proteins derived from SMP1-1-FLAG-TurboID parasites. This
278 approach yielded 218 flagellar candidates in epimastigotes and 99 proteins in
279 amastigotes, where 40 proteins were common to both *T. cruzi* life stages. Flagellar
280 localization was confirmed for a subset of proteins in this dataset, based on
281 endogenous epitope-tagging, and many more were predicted based on demonstrated
282 localization in the related trypanosomatids, *T. brucei* or *Leishmania spp*.

283 The functional capabilities of the *T. cruzi* flagellum are broadly uncharacterized,
284 beyond its role in propelling motile life stages and anchoring epimastigotes to the rectal
285 mucosa in the insect vector [4,45,46]. However, the recent recognition that the flagellum of
286 cytosolically-localized intracellular amastigotes is capable of beating and establishes
287 physical contact with host mitochondria [3,6], points to a potential role for the amastigote
288 flagellum in host environmental sensing. Although little is known regarding the sensory
289 capabilities of trypanosomatids in general, significant progress has been made toward a
290 molecular understanding of pH taxis and social motility in the insect stages of *T. brucei*
291 [21,23]. The sensory system involves regulation of cyclic AMP levels, modulated by

292 flagellar receptor-type adenylate cyclases and cyclic AMP phosphodiesterases[22] and
293 the involvement of a cyclic AMP responsive protein (CARP3), which is thought to act in
294 a complex with adenylate cyclases [20]. Our discovery, that CARP3 is expressed in the
295 replicative stages of *T. cruzi,* including intracellular amastigotes (despite the inability to
296 localize the tagged protein in this life stage), is quite exciting given the established role
297 of CARP3 in *T. brucei* [20]*.* In *T. brucei* CARP3 is known to co-localize with calpain 1.3 at
298 the distal region of the flagellum, where the two proteins may physically interact [20]. We
299 show that the calpain 1.3 ortholog is also expressed in the flagellum of *T. cruzi,* where it
300 localizes exclusively to the flagellar tip in intracellular amastigotes, a recognized
301 signaling domain in trypanosomatids [33(p2),47]. Calpain 1.3 belongs to a sub-family of
302 cysteine peptidases that are predicted to be catalytically inactive as they lack one or
303 more of the active site amino acid residues [48]. Proteins with these features are thought
304 to play a role in calcium homeostasis / signaling, including the calcium-based regulation
305 of adenylate cyclase complexes [20,49]. Despite the lack of social motility in *T. cruzi,* the
306 expression of flagellar CARP3 and calpain 1.3 in this species is a strong indicator that
307 the *T. cruzi* flagellum is equipped to sense and integrate signals from the environment.
308 Dissection of the functional roles of CARP3 and calpain 1.3 in *T. cruzi* is expected to be
309 instrumental in establishing the existence of flagellum-based environmental sensing in
310 this parasite. In addition, a functional investigation of the hypothetical protein
311 (TcCLB.509965.20) that also localizes to the distal end of the *T. cruzi* flagellum but
312 lacks an obvious ortholog in *T. brucei* or *Leishmania*, has the potential to reveal novel
313 biological or mechanistic insights into the role of the *T. cruzi* flagellum in different life
314 stages.

315 The proteomic datasets generated here offer new opportunities to pursue the
316 localization and functional analyses of many uncharacterized proteins, some of which
317 are unique to the *T. cruzi* lineage. While some of the annotated proteins are not
318 predicted to localize to the flagellum (based on annotation and TrypTag localization),
319 including proteins involved in protein trafficking which may have encountered SMP1-1-
320 FLAG-TurboID *en route* to the flagellum, there are a number of proteins with
321 transmembrane domains or N-myristoylation consensus sequences that predict
322 membrane-association. SMP-1 contains the N-myristoylation sequence motif
323 (MGXXXS/T) known to direct flagellar localization and tethering to the inner flagellar
324 membrane in *Leishmania*, where it associates tightly with detergent-resistant
325 membranes (lipid rafts) [41] and forms homodimers [41]. As such, SMP1-1 may
326 preferentially interact with other membrane proteins associated with lipid rafts in the
327 flagellar membrane. It is notable that a number of proteins that were among the
328 strongest 'hits' in the flagellar candidate pool, such as calpain 1.3 and CARP3, also
329 have MGXXXS/T motifs. While this motif is insufficient to direct a protein to the flagellum
330 [41], proteins with lipid anchoring motifs or transmembrane domains could be prioritized
331 for future studies of the *T. cruzi* flagellum. Notably, we did not identify adenylate
332 cyclases in our data, even though CARP3 and calpain 1.3 were identified in a proximity-
333 labeling study in *T. brucei* designed to identify flagellar tip proteins that interact with
334 adenylate cyclase 1 [33]. While the proximity-dependent labeling approach used in this
335 study enabled the discovery of a subset of flagellar proteins in *T. cruzi* amastigotes
336 (where physical isolation of the short amastigote flagellum may not be feasible), it is
337 understood that the resulting proteomes derived for the two parasite life stages are not

338 comprehensive and many *T. cruzi* flagellar membrane proteins remain to be identified.
339 With the discovery of additional flagellar proteins in *T. cruzi,* opportunities will be
340 presented to use one or more of these proteins as alternative bait proteins for proximity
341 labeling with a view to expanding the flagellar proteome in this understudied parasite.

342 Overall, we have presented the first use of proximity-dependent biotinylation in *T.*
343 *cruzi* for the identification of more than 200 candidate flagellar proteins across two
344 parasite life stages, thereby creating an important resource for the research community.
345 As more information becomes available for the *T. cruzi* amastigote flagellum, it is
346 expected to provide some context for the biological role of the flagellum in infection and
347 these interactions may be the key for specific targeting of parasite function and viability
348 within the mammalian host. Future investigation focused on identifying the function of
349 potential sensory flagellar candidates in *T. cruzi* epimastigote and amastigote flagella,
350 may aid in the discovery of these currently unknown host-parasite interaction
351 mechanisms.

352

353 **Methods and Materials**

354 **Reagents**

355 Compounds were purchased and diluted to stock concentrations: Biotin, 100 mM in
356 DMSO (Sigma Aldrich, St. Louis, Missouri, USA). Phenylmethylsulfonyl fluoride (PMSF),
357 10 mM in isopropanol (Sigma Aldrich, St. Louis, Missouri, USA). Tosyl-L-lysyl-
358 chloromethane hydrochloride (TLCK), 5 mM in DMSO (Abcam, Cambridge, United
359 Kingdom).

360

361 **Mammalian cell culture**

362 Normal Human Neonatal Dermal Fibroblasts (NHDF; Lonza, Basel, Switzerland) and
363 monkey kidney epithelial cells (LLC-MK2; American Type Culture Collection) were
364 maintained in Dulbecco's modified Eagle medium (DMEM; HyClone, Logan, Utah, USA)
365 supplemented with 10% heat-inactivated FBS (Gibco, Waltham, Massachusetts, USA),
366 25 mM glucose, 2 mM L-glutamine, and 100 U/mL penicillin-streptomycin (DMEM-10) at
367 37°C and 5% CO_2.

368

369 **Growth and maintenance of *T. cruzi***

370 *Trypanosoma cruzi* Tulahuén LacZ clone C4 was obtained from the American Type
371 Culture Collection (ATCC, PRA-330; ATCC, Manassas, Virginia, USA). The
372 epimastigote stage was propagated at 28°C in liver infusion tryptose (LIT) medium
373 (4 g/L NaCl, 0.4 g/L KCl, 8 g/L Na2HPO4, 2 g/L dextrose, 3 g/L liver infusion broth, 5 g/L
374 tryptose, with 25 mg/L hemin and 10% heat-inactivated FBS). The mammalian cell
375 infection cycle was initiated with metacyclic trypomastigotes arising within stationary
376 phase epimastigote cultures that were shifted from LIT to DMEM + 2% FBS (DMEM-2)
377 for 5 days at 28°C. Metacyclic-enriched cultures were washed in DMEM-2 and
378 incubated with confluent LLC-MK2 monolayers at 37°C, 5% CO_2 to allow invasion.
379 Mammalian stage trypomastigotes that emerged from infected LLC-MK2 cells (within 5-
380 10 days) were harvested from culture supernatants and used to infect fresh LLC-MK2
381 monolayers. This cycle was continued on weekly basis to maintain the mammalian-
382 infective stages of *T. cruzi* in culture. For experimental infections, trypomastigotes
383 collected from LLC-MK2 maintenance cultures were pelleted at 2060 x g for 10 minutes

384 and pellets were incubated at 37°C, 5% CO_2 for 2-4 hours to allow motile
385 trypomastigotes to swim up into the supernatant. Purified trypomastigotes in the
386 supernatant were collected, washed once in DMEM-2 and utilized to infect sub-
387 confluent monolayers of NHDF as indicated.
388
389 **Generation of stable *T. cruzi* transfectants**
390 *T. cruzi* strains expressing TcSMP1-1GFP were previously generated [6]. A plasmid
391 containing the TurboID sequence was a kind gift of Jeffrey Dvorin (Harvard Medical
392 School). Each TurboID construct was used to replace the GFP-P2A-puro cassette in a
393 modified pTREX plasmid [50,51] containing either SMP1-1-GFP or GFP alone. The inserts
394 in the pTREX backbone to generate the F-Turbo plasmids were SMP1-1-TurboID-P2A-
395 puro (F-Turbo-P) or SMP-1-1-TurboID-T2A-puro (F-Turbo-T). The inserts and backbone
396 were assembled using the NEB HiFi DNA assembly kit (New England Biolabs, Ipswich,
397 Massachusetts, USA), resulting in the final plasmids. For the cytosolic control, TurboID-
398 P2A-puro was amplified using PCR and then inserted into the pTREX-GFP backbone,
399 replacing GFP between the SpeI and XmaI cut sites using or through restriction enzyme
400 cloning. To generate TurboID-expressing parasites *T. cruzi* epimastigotes were
401 transfected with 15 µg of the respective DNA. Prior to transfection log-phase *T. cruzi*
402 epimastigotes, were pelleted at 2060 x g for 10 minutes, resuspended in 100 µL of Tb
403 BSF buffer [52] ($4x10^7$ parasites) and placed into a sterile 2 mm gap cuvette with the
404 appropriate DNA and transfected using an Amaxa Nucleofector II (Lonza, Basel,
405 Switzerland; U-33 program). Parasites were immediately transferred to LIT medium for

406 24 hours before adding 10 μg/mL puromycin (Invivogen, San Diego, California, USA) or
407 50 μg/mL blasticidin (Invivogen, San Diego, California, USA) for selection.
408
409 CRISPR/Cas9-facilitated epitope tagging of genomic loci in *T. cruzi* was performed as
410 described [53]. Briefly, each gene of interest was PCR-amplified from genomic DNA (*T.*
411 *cruzi* Tulahuen strain) and PCR products sequenced. Two gRNA binding sites near the
412 3' region of each gene of interest were identified using EuPaGDT [54]. Editing of the
413 previously modified pTREX-n-Cas9 plasmid [51] (Addgene plasmid 68708), performed to
414 exchange the previous gRNA sequence was achieved using a Q5 mutagenesis kit (New
415 England Biolabs, Ipswich, Massachusetts, USA). gRNA sequences were inserted into
416 pTREX-n-Cas9 using primers specific to the gene of interest in **Supplementary Table**
417 **4**, such that the previous gRNA sequence was replaced. The template for generating
418 homology-directed repair DNA for gene tagging was constructed by inserting a P2A viral
419 skip peptide in frame with a downstream blasticidin-S deaminase (BSD) or puromycin
420 N-acetyl-transferase (puro) and TOPO cloned into a pCR4 backbone (Thermo Fisher,
421 Waltham, MA, United States of America) [51]. Homology template was amplified from this
422 template using ultramer pairs (**Supplementary Table 4**) that provided 100 bp of
423 homology for the gene of interest, the FLAG tag and 20 bp of homology to template.
424 Parasite were transfected as above with 25 μg of each gRNA-specific pTREX-n-Cas9
425 plasmid to the gene of interest and 50 μg of homology repair template. Correct
426 integration of the endogenous tag and drug cassette was established via PCR
427 (**Supplementary Fig. 2**).
428

429 **Detection of biotinylated protein fractions in *T. cruzi***

430 *Epimastigotes*: 1.5 x 10^8 epimastigotes were pelleted at 2060 x g for 10 minutes,
431 resuspended in 1 ml of LIT and incubated with 50 µM biotin for 10 minutes at 37°C.
432 Parasites were washed twice with ice-cold PBS then resuspended in 1 ml cell lysis
433 buffer [55] (0.5% Nonidet P-40, 500 mM NaCl, 5 mM EDTA, 1 mM DTT, 50 mM Tris-Base,
434 0.4% SDS, pH 7.4) with Roche cOmplete™ Protease Inhibitor (Sigma-Aldrich, St. Louis,
435 Missouri, USA), 100 µM PMSF and 10 µM TLCK. Lysates were sonicated using 3
436 pulses of 30 seconds at 100% amplitude (Q700 sonicator, QSONICA, Newton,
437 Connecticut), with 15 sec breaks between to cool the tubes on ice. Samples were
438 centrifuged at 16,000 x g for 20 minutes at 4°C and the supernatant was collected.
439 Aliquots of clarified lysate (3 x 10^6 parasite equivalents) were resolved by SDS-PAGE
440 (Mini-PROTEAN®TGX protein gel; Bio-Rad, Hercules, California, USA), transferred to
441 PVDF membrane (Immobilon®-FL, MilliporeSigma, Burlington, Massachusetts, USA)
442 and probed with Streptavidin DyLight™ 800 (Thermo Fisher Scientific, Waltham,
443 Massachusetts, USA) to detect biotinylated proteins.

444

445 *Intracellular amastigotes*: At 48 hpi, *T. cruzi*-infected NHDF monolayers in T-150 flasks
446 were exposed to 100 µM biotin for 10 minutes at 37°C, 5% CO_2. Monolayers were then
447 rinsed three times with cold PBS and incubated with 2 mL of cell lysis buffer (as above).
448 Flasks were agitated manually for 5 minutes then cells were scraped and transferred
449 into a tube containing 0.5 µL of benzonase (Sigma-Aldrich, St. Louis, Missouri, USA).
450 Tubes were placed on a rotative wheel for 15 minutes at room temperature, then
451 sonicated as above. Amastigote loading volumes were normalized via Western blot as

452 follows. Equal volumes of serially diluted protein lysates, generated for WT, F-Turbo
453 and C-Turbo infected NHDF, were resolved by SDS-PAGE (Mini-PROTEAN®TGX gels),
454 transferred to PVDF membrane and probed with a rabbit antibody to trypanosome BiP
455 [56], followed by α-Rabbit Alexa Flour 647. A LiCor Odessy® CLx imager was used to
456 measure BiP signal in each sample (Image Studio). Relative BiP densities were used to
457 adjust the volumes of each amastigote lysates (confirmed by independent western
458 blots) prior to loading on streptavidin beads.
459
460 **Isolation of biotinylated proteins**
461 Protein lysates were loaded onto Pierce™ High-Capacity Streptavidin Agarose (Thermo
462 Fisher Scientific, Waltham, Massachusetts, USA). 100 µL and 150 µL packed bead
463 volumes were used for epimastigote and amastigote samples, respectively, and
464 incubated on a rotative wheel overnight at 4°C. For all following steps, washes
465 consisted of adding 1 mL of the indicated buffer and placing the tube on the rotative
466 wheel for 5 minutes, then spinning down the agarose beads for 1 minute at 500 x g, as
467 previously described [55]. Beads with bound protein were subjected to 5 washes with
468 Buffer 1 (8 M urea, 200 mM NaCl, 100 mM Tris, pH 8.0) with 0.2% sodium dodecyl
469 sulfate (SDS), 5 washes with Buffer 1 containing 2% SDS, and 5 washes with Buffer 1
470 with no SDS were completed at room temperature. Next, 2 washes with 200 mM NaCl,
471 100 mM Tris, at a pH of 7.0 and 2 washes with Tris, pH 8.0 were completed at 4°C.
472 Washed beads were adjusted to pH 7.5 with 200 mM HEPES (4-(2-hydroxyethyl)-1-
473 piperazineethanesulfonic acid) and bound proteins were reduced using 5 mM
474 dithiothreitol (Sigma-Aldrich) at 37°C for 1 h, followed by alkylation of cysteine residues

475 using 15 mM iodoacetamide (Sigma-Aldrich) in the dark at room temperature for 1 h.
476 Excessive iodoacetamide was quenched using 10 mM dithiotheritol. Protein mixtures
477 were diluted in 1:6 ratio (v/v) using ultrapure water prior to digestion using sequencing
478 grade trypsin (Promega) at 37°C for 16 h. Digested peptides were subsequently
479 desalted using self-packed C18 STAGE tips (3M EmporeTM) [57] for LC-MS/MS analysis.
480

481 **Mass spectrometry**

482

483 *Epimastigotes*: Desalted peptides were resuspended in 0.1% (v/v) formic acid and
484 loaded onto HPLC-MS/MS system for analysis on an Orbitrap Q-Exactive Exploris 480
485 (Thermo Fisher Scientific) mass spectrometer coupled to an Easy nanoLC 1000
486 (Thermo Fisher Scientific) with a flow rate of 250 nl/min. The stationary phase buffer
487 was 0.5 % formic acid and mobile phase buffer was 0.5 % (v/v) formic acid in
488 acetonitrile. Chromatography for peptide separation was performed using increasing
489 organic proportion of acetonitrile (5 – 40 % (v/v)) over a 120 min gradient) on a self-
490 packed analytical column using PicoTipTM emitter (New Objective, Woburn, MA) using
491 Reprosil Gold 120 C-18, 1.9 µm particle size resin (Dr. Maisch, Ammerbuch-Entringen,
492 Germany). The mass spectrometry analyzer operated in data dependent acquisition
493 mode with a top ten method at a mass range of 300–2000 Da. Data were processed
494 using MaxQuant software (version 1.5.2.8) [58] with the following setting: oxidized
495 methionine residues and protein N-terminal acetylation as variable modification,
496 cysteine carbamidomethylation as fixed modification, first search peptide tolerance 20
497 ppm, main search peptide tolerance 4.5 ppm. Protease specificity was set to trypsin

498 with up to 2 missed cleavages allowed. Only peptides longer than five amino acids were
499 analyzed, and the minimal ratio count to quantify a protein is 2 (proteome only). The
500 false discovery rate (FDR) was set to 1% for peptide and protein identifications.
501 Database searches were performed using the Andromeda search engine integrated into
502 the MaxQuant environment [59] against the UniProt *Trypanosoma cruzi* strain CL Brener
503 (352153) database containing 19,242 entries (March 2020). "Matching between runs"
504 algorithm with a time window of 0.7 min was employed to transfer identifications
505 between samples processed using the same nanospray conditions. Protein tables were
506 filtered to eliminate identifications from the reverse database and common
507 contaminants.
508
509 *Amastigotes*: Desalted peptides were resolubilized in 0.1% (v/v) formic acid and loaded
510 onto HPLC-MS/MS system for analysis on an Orbitrap Q-Exactive Exploris 480 (Thermo
511 Fisher Scientific) mass spectrometer coupled to an FAIMS Pro Interface system and
512 Easy nanoLC 1000 (Thermo Fisher Scientific) with a flow rate of 300 nl/min. The
513 stationary phase buffer was 0.1 % formic acid, and mobile phase buffer was 0.1 % (v/v)
514 formic acid in 80% (v/v) acetonitrile. Chromatography for peptide separation was
515 performed using increasing organic proportion of acetonitrile (5 – 40 % (v/v)) over a 120
516 min gradient) on a self-packed analytical column using PicoTip™ emitter (New
517 Objective, Woburn, MA) using Reprosil Gold 120 C-18, 1.9 µm particle size resin (Dr.
518 Maisch, Ammerbuch-Entringen, Germany). High precision iRT calibration was used for
519 samples processed using the same nanospray conditions [60]. The mass spectrometry
520 analyzer operated in data independent acquisition mode at a mass range of 300–

521 2000 Da, compensation voltages of -50/-70 CVs with survey scan of 120,000 and
522 15,000 resolutions at MS1 and MS2 levels, respectively. Data were processed using
523 Spectronaut™ software (version 15; Biognosys AG) [61] using directDIA™ analysis with
524 default settings, including: oxidized methionine residues, biotinylation, protein N-
525 terminal acetylation as variable modification, cysteine carbamidomethylation as fixed
526 modification, initial mass tolerance of MS1 and MS2 of 15 ppm. Protease specificity was
527 set to trypsin with up to 2 missed cleavages were allowed. Only peptides longer than
528 seven amino acids were analyzed, and the minimal ratio count to quantify a protein is 2
529 (proteome only). The false discovery rate (FDR) was set to 1% for peptide and protein
530 identifications. Database searches were performed against the UniProt *Trypanosoma*
531 *cruzi* strain CL Brener (352153) database containing 19,242 entries (March 2020).
532 Protein tables were filtered to eliminate identifications from the reverse database and
533 common contaminants.
534
535 **Principal component analysis**
536 All protein intensity scores were uploaded to Metaboanalyst 5.0 [62] to perform statistical
537 analysis, with one factor. Data was entered as peak intensities and filtered using the
538 interquartile range, then normalized by sum and log transformed. 2D PCA scores were
539 plotted in Prism GraphPad.
540
541 **Volcano plots**
542 For epimastigote data, protein intensity scores for all proteins that were found to be 100-
543 fold or higher enriched in the F-Turbo or C-Turbo samples over wild type were loaded

544 into Prism GraphPad, and Log_{10} transformed. Multiple unpaired t-tests were run on the
545 data with a false discovery rate of 1% and the results were reported as F-Turbo – C-
546 Turbo, with -log10(q value) reported for the volcano plot. For amastigote data,
547 Spectronaut™ software was used to generate the statistical analysis of the amastigote
548 proteomics. Within the DIA analysis pipeline, the default settings were used, including a
549 false discovery rate of 1% and a n unpaired Student's t-test was performed. Fold
550 changes were reported as an average Log10 (epimastigotes) or Log2 (amastigotes)
551 ratio for the volcano plot. Volcano plot was created in Prism GraphPad. Post-analysis,
552 six proteins were excluded from the amastigote flagellar enriched list, as they were not
553 identified in 2 of 3 biological replicates. Additionally, all allelic duplicates were removed
554 to ensure that the proteins listed in the final tables were represented by a single gene
555 identifier corresponding to the CL Brener reference genome (TriTrypDB;
556 https://tritrypdb.org/), but paralogs remain.
557

558 **Interpro domain enrichment analysis**

559 DAVID [63] enrichment was used to assign Interpro domains to all of the proteins found
560 to be significantly enriched in either of the F-Turbo samples. No weighting of the data
561 was completed. Interpro domains with a p-value ≤ 0.05 were considered significantly
562 enriched.
563

564 **Indirect immunofluorescence microscopy**

565 Epimastigotes were fixed directly in growth medium with the addition of
566 paraformaldehyde (1% final concentration in PBS) for 10-minute at 4°C. Fixed parasites

567 were pelleted by centrifuging for 10 minutes at 4000 x g and resuspended in PBS. 10 µL
568 of the parasite solution was dropped onto poly-L-lysine coated slides and allowed to dry
569 completely prior to staining. For immunostaining of intracellular amastigotes, *T. cruzi*-
570 infected NHDF on round cover glass (12 mm, #1.5; Electron Microscopy Sciences,
571 Hatfield, Pennsylvania, USA) were fixed at 48 hours post-infection with 1% (v/v)
572 paraformaldehyde/PBS. All steps of the immunostaining protocol were preceded by
573 three washes with PBS and carried out at room temperature. Parasites were
574 permeabilized with a 0.1% Triton-X 100 solution (JT Baker, Phillipsburg, New Jersey,
575 USA) for 10 minutes and blocked with 3% BSA (Sigma-Aldrich, St. Louis, Missouri,
576 USA) in PBS for 1 hour. The primary antibody solution containing 1:400 mouse α-FLAG
577 (clone M2, Sigma-Aldrich, St. Louis, Missouri, USA) and/or 1:1,500 rabbit α-FCaBP [64] in
578 1% BSA in PBS was added for 1 hour, followed by a 1:1000 α-Mouse Alexa Flour 594
579 and/or α-Rabbit Alexa Flour 647 solution in 1% BSA in PBS for 1 hour. DAPI (0.2
580 µg/mL; Thermo Fisher Scientific, Waltham, Massachusetts, USA) in PBS was added for
581 5 minutes, and following washes, coverslips were placed onto slides with Prolong®
582 Diamond mountant (Thermo Fisher Scientific, Waltham, Massachusetts, USA). After
583 setting for 24 hours parasites were imaged using a Yokogawa CSU-X1 spinning disk
584 confocal system paired with a Nikon Ti-E inverted microscope and an iXon Ultra 888
585 EMCCD camera (100X objective). Image processing, analysis, and display were
586 performed using ImageJ Fiji software [65].
587

588 **Acknowledgments**

We thank the Sabri Ülker Center's Advanced Imaging Lab at the Harvard T.H. Chan School of Public Health for microscopy training and access. Additionally, we would like to thank Zon Weng Lai from the Harvard Chan Advanced Multi-omics Platform at the Harvard T.H. Chan School of Public Health for his assistance in interpreting the mass spectrometry data. We thank Jeffrey Dvorin (Boston Children's Hospital) for providing the TurboID plasmid, David Engman (Cedars-Sinai Medical Center) for the gift of the anti-FCaBP antibody and Jay Bangs (The State University of New York at Buffalo) for anti-BiP antibody. We also thank Lucas Pagura for his thoughtful discussion. This work was supported by NIH grant R21AI135520 awarded to BAB and NIH training grant 5T32AI049928.

Competing interests

No competing interests declared.

References

1. Bern C. Chagas' Disease. *N Engl J Med*. 2015;373(5):456-466. doi:10.1056/NEJMra1410150

2. Stanaway JD, Roth G. The burden of Chagas disease: estimates and challenges. *Glob Heart*. 2015;10(3):139-144. doi:10.1016/j.gheart.2015.06.001

3. Lentini G, Dos Santos Pacheco N, Burleigh BA. Targeting host mitochondria: A role for the *Trypanosoma cruzi* amastigote flagellum. *Cell Microbiol*. 2018;20(2). doi:10.1111/cmi.12807

4. Nogueira NFS, Gonzalez MS, Gomes JE, de Souza W, Garcia ES, Azambuja P, Nohara LL, Almeida IC, Zingales B, Colli W. *Trypanosoma cruzi*: involvement of glycoinositolphospholipids in the attachment to the luminal midgut surface of Rhodnius prolixus. *Exp Parasitol*. 2007;116(2):120-128. doi:10.1016/j.exppara.2006.12.014

5. Schmidt J, Kleffmann T, Schaub GA. Hydrophobic attachment of *Trypanosoma cruzi* to a superficial layer of the rectal cuticle in the bug *Triatoma infestans*. *Parasitol Res*. 1998;84(7):527-536. doi:10.1007/s004360050443

6. Won MM, Krüger T, Engstler M, Burleigh BA. The intracellular amastigote of *Trypanosoma cruzi* maintains an actively beating flagellum. *mBio*. In Press.

7. Gonçalves CS, Ávila AR, de Souza W, Motta MCM, Cavalcanti DP. Revisiting the *Trypanosoma cruzi* metacyclogenesis: morphological and ultrastructural analyses during cell differentiation. *Parasit Vectors*. 2018;11:83. doi:10.1186/s13071-018-2664-4

8. Gadelha C, Wickstead B, McKean PG, Gull K. Basal body and flagellum mutants reveal a rotational constraint of the central pair microtubules in the axonemes of trypanosomes. *J Cell Sci*. 2006;119(Pt 12):2405-2413. doi:10.1242/jcs.02969

9. Gardiner PJ. Pellicle-associated structures in the amastigote stage of *Trypanosoma cruzi* and *Leishmania* species. *Ann Trop Med Parasitol*. 1974;68(2):167-176. doi:10.1080/00034983.1974.11686935

10. Portman N, Gull K. The paraflagellar rod of kinetoplastid parasites: From structure to components and function. *Int J Parasitol*. 2010;40(2):135. doi:10.1016/j.ijpara.2009.10.005

11. Kelly FD, Sanchez MA, Landfear SM. Touching the Surface: Diverse Roles for the Flagellar Membrane in Kinetoplastid Parasites. *Microbiol Mol Biol Rev MMBR*. 2020;84(2):e00079-19. doi:10.1128/MMBR.00079-19

12. Gluenz E, Höög JL, Smith AE, Dawe HR, Shaw MK, Gull K. Beyond 9+0: noncanonical axoneme structures characterize sensory cilia from protists to humans. *FASEB J Off Publ Fed Am Soc Exp Biol*. 2010;24(9):3117-3121. doi:10.1096/fj.09-151381

13. Kelly FD, Yates PA, Landfear SM. Nutrient Sensing in *Leishmania*: Flagellum and Cytosol. *Mol Microbiol*. Published online October 28, 2020. doi:10.1111/mmi.14635

14. Saegusa Y, Yoshimura K. cAMP controls the balance of the propulsive forces generated by the two flagella of *Chlamydomonas*. *Cytoskelet Hoboken NJ*. 2015;72(8):412-421. doi:10.1002/cm.21235

15. Bickerton P, Sello S, Brownlee C, Pittman JK, Wheeler GL. Spatial and temporal specificity of Ca2+ signalling in *Chlamydomonas reinhardtii* in response to osmotic stress. *New Phytol*. 2016;212(4):920-933. doi:10.1111/nph.14128

16. Christensen ST, Pedersen LB, Schneider L, Satir P. Sensory cilia and integration of signal transduction in human health and disease. *Traffic*. 2007;8(2):97-109. doi:10.1111/j.1600-0854.2006.00516.x

17. Camara M de los M, Bouvier LA, Miranda MR, Pereira CA. The flagellar adenylate kinases of *Trypanosoma cruzi*. *FEMS Microbiol Lett*. 2015;362(1):1-5. doi:10.1093/femsle/fnu020

18. Langousis G, Hill KL. Motility and more: the flagellum of *Trypanosoma brucei*. *Nat Rev Microbiol*. 2014;12(7):505-518. doi:10.1038/nrmicro3274

19. Peacock L, Bailey M, Carrington M, Gibson W. Meiosis and haploid gametes in the pathogen *Trypanosoma brucei*. *Curr Biol CB*. 2014;24(2):181-186. doi:10.1016/j.cub.2013.11.044

20. Bachmaier S, Giacomelli G, Calvo-Alvarez E, Vieira LR, Abbeele JVD, Aristodemou A, Lorentzen E, Gould M, Brennand A, Dupuy JW, Forné I, imhof A, Bramkamp M, Salmon D, Rotureau B, Boshart M. A multi-adenylate cyclase regulator at the flagellar tip controls African trypanosome transmission. Published online 2022. doi:10.21203/rs.3.rs-1216579/v1

21. Shaw S, Knüsel S, Abbühl D, Naguleswaran A, Etzensperger R, Benninger M, Roditi I. Cyclic AMP signalling and glucose metabolism mediate pH taxis by African trypanosomes. *Nat Commun*. 2022;13(1):603. doi:10.1038/s41467-022-28293-w

22. Oberholzer M, Saada EA, Hill KL. Cyclic AMP Regulates Social Behavior in African Trypanosomes. *mBio*. 2015;6(3):e01954-14. doi:10.1128/mBio.01954-14

23. Lopez MA, Saada EA, Hill KL. Insect stage-specific adenylate cyclases regulate social motility in African trypanosomes. *Eukaryot Cell*. 2015;14(1):104-112. doi:10.1128/EC.00217-14

24. Figarella K, Uzcategui NL, Zhou Y, LeFurgey A, Ouellette M, Bhattacharjee H, Mukhopadhyay R. Biochemical characterization of *Leishmania major* aquaglyceroporin LmAQP1: possible role in volume regulation and osmotaxis. *Mol Microbiol*. 2007;65(4):1006-1017. doi:10.1111/j.1365-2958.2007.05845.x

25. Rodriguez-Contreras D, Aslan H, Feng X, Tran K, Yates PA, Kamhawi S, Landfear SM. Regulation and biological function of a flagellar glucose transporter in *Leishmania mexicana*: a potential glucose sensor. *FASEB J Off Publ Fed Am Soc Exp Biol*. 2015;29(1):11-24. doi:10.1096/fj.14-251991

26. Piper RC, Xu X, Russell DG, Little BM, Landfear SM. Differential targeting of two glucose transporters from *Leishmania enriettii* is mediated by an NH2-terminal domain. *J Cell Biol*. 1995;128(4):499-508. doi:10.1083/jcb.128.4.499

27. Goldman-Pinkovich A, Kannan S, Nitzan-Koren R, Puri M, Pawar H, Bar-Avraham Y, McDonald J, Sur A, Zhang WW, Matlashewski G, Madhubala R, Michaeli S, Myler PJ, Zilberstein D. Sensing Host Arginine Is Essential for *Leishmania* Parasites' Intracellular Development. *mBio*. 2020;11(5). doi:10.1128/mBio.02023-20

28. Oberholzer M, Langousis G, Nguyen HT, Saada EA, Shimogawa MM, Jonsson ZO, Nguyen SM, Wohlschlegel JA, Hill KL. Independent Analysis of the Flagellum Surface and Matrix Proteomes Provides Insight into Flagellum Signaling in

Mammalian-infectious *Trypanosoma brucei*. *Mol Cell Proteomics MCP*. 2011;10(10):M111.010538. doi:10.1074/mcp.M111.010538

29. Beneke T, Demay F, Hookway E, Ashman N, Jeffery H, Smith J, Valli J, Becvar T, Myskova J, Lestinova T, Shafiq S, Sadlova J, Volf P, Wheeler RJ, Gluenz E. Genetic dissection of a *Leishmania* flagellar proteome demonstrates requirement for directional motility in sand fly infections. *PLOS Pathog*. 2019;15(6):e1007828. doi:10.1371/journal.ppat.1007828

30. Subota I, Julkowska D, Vincensini L, Reeg N, Buisson J, Blisnick T, Huet D, Perrot S, Santi-Rocca J, Duchateau M, Hourdel V, Rousselle JC, Cayet N, Namane A, Chamot-Rooke J, Bastin P. Proteomic analysis of intact flagella of procyclic *Trypanosoma brucei* cells identifies novel flagellar proteins with unique sub-localization and dynamics. *Mol Cell Proteomics MCP*. 2014;13(7):1769-1786. doi:10.1074/mcp.M113.033357

31. Broadhead R, Dawe HR, Farr H, Griffiths S, Hart SR, Portman N, Shaw MK, Ginger ML, Gaskell SJ, McKean PG, Gull K. Flagellar motility is required for the viability of the bloodstream trypanosome. *Nature*. 2006;440(7081):224-227. doi:10.1038/nature04541

32. Hu H, Zhou Q, Li Z. SAS-4 Protein in *Trypanosoma brucei* Controls Life Cycle Transitions by Modulating the Length of the Flagellum Attachment Zone Filament. *J Biol Chem*. 2015;290(51):30453-30463. doi:10.1074/jbc.M115.694109

33. Vélez-Ramírez DE, Shimogawa MM, Ray SS, Lopez A, Rayatpisheh S, Langousis G, Gallagher-Jones M, Dean S, Wohlschlegel JA, Hill KL. APEX2 Proximity Proteomics Resolves Flagellum Subdomains and Identifies Flagellum Tip-Specific Proteins in *Trypanosoma brucei*. *mSphere*. 2021;6(1):e01090-20. doi:10.1128/mSphere.01090-20

34. Branche C, Kohl L, Toutirais G, Buisson J, Cosson J, Bastin P. Conserved and specific functions of axoneme components in trypanosome motility. *J Cell Sci*. 2006;119(16):3443-3455. doi:10.1242/jcs.03078

35. Jimenez V, Docampo R. Molecular and Electrophysiological Characterization of a Novel Cation Channel of *Trypanosoma cruzi*. *PLOS Pathog*. 2012;8(6):e1002750. doi:10.1371/journal.ppat.1002750

36. Engman DM, Krause KH, Blumin JH, Kim KS, Kirchhoff LV, Donelson JE. A novel flagellar Ca2+-binding protein in trypanosomes. *J Biol Chem*. 1989;264(31):18627-18631.

37. Maric D, McGwire BS, Buchanan KT, Olson CL, Emmer BT, Epting CL, Engman DM. Molecular Determinants of Ciliary Membrane Localization of *Trypanosoma cruzi* Flagellar Calcium-binding Protein. *J Biol Chem*. 2011;286(38):33109-33117. doi:10.1074/jbc.M111.240895

38. Buchanan KT, Ames JB, Asfaw SH, Wingard JN, Olson CL, Campana PT, Araújo APU, Engman DM. A flagellum-specific calcium sensor. *J Biol Chem*. 2005;280(48):40104-40111. doi:10.1074/jbc.M505777200

39. Maldonado RA, Mirzoeva S, Godsel LM, Lukas TJ, Goldenberg S, Watterson DM, Engman DM. Identification of calcium binding sites in the trypanosome flagellar calcium-acyl switch protein. *Mol Biochem Parasitol*. 1999;101(1-2):61-70. doi:10.1016/s0166-6851(99)00055-9

40. Branon TC, Bosch JA, Sanchez AD, Udeshi ND, Svinkina T, Carr SA, Feldman JL, Perrimon N, Ting AY. Efficient proximity labeling in living cells and organisms with TurboID. *Nat Biotechnol*. 2018;36(9):880-887. doi:10.1038/nbt.4201

41. Tull D, Naderer T, Spurck T, Mertens HDT, Heng J, McFadden GI, Gooley PR, McConville MJ. Membrane protein SMP-1 is required for normal flagellum function in *Leishmania*. *J Cell Sci*. 2010;123(Pt 4):544-554. doi:10.1242/jcs.059097

42. Dean S, Sunter JD, Wheeler RJ. TrypTag.org: A Trypanosome Genome-wide Protein Localisation Resource. *Trends Parasitol*. 2017;33(2):80-82. doi:10.1016/j.pt.2016.10.009

43. Calvo-Álvarez E, Bonnefoy S, Salles A, Benson FE, McKean PG, Bastin P, Rotureau B. Redistribution of FLAgellar Member 8 during the trypanosome life cycle: Consequences for cell fate prediction. *Cell Microbiol*. 2021;23(9):e13347. doi:10.1111/cmi.13347

44. Tetaud E, Lefebvre M, M'Bang-Benet DE, Crobu L, Blancard C, Sterkers Y, Pages M, Bastien P, Merlin G. TbFlabarin, a flagellar protein of *Trypanosoma brucei*, highlights differences between *Leishmania* and *Trypanosoma* flagellar-targeting signals. *Exp Parasitol*. 2016;166:97-107. doi:10.1016/j.exppara.2016.04.004

45. Kollien A, Schaub G. The Development of *Trypanosoma cruzi* in Triatominae. *Parasitol Today*. 2000;16(9):381-387. doi:10.1016/S0169-4758(00)01724-5

46. Cámara M de los M, Balouz V, Centeno Cameán C, Cori CR, Kashiwagi GA, Gil SA, Macchiaverna NP, Cardinal MV, Guaimas F, Lobo MM, de Lederkremer RM, Gallo-Rodriguez C, Buscaglia CA. *Trypanosoma cruzi* surface mucins are involved in the attachment to the *Triatoma infestans* rectal ampoule. *PLoS Negl Trop Dis*. 2019;13(5):e0007418. doi:10.1371/journal.pntd.0007418

47. Varga V, Moreira-Leite F, Portman N, Gull K. Protein diversity in discrete structures at the distal tip of the trypanosome flagellum. *Proc Natl Acad Sci U S A*. 2017;114(32):E6546-E6555. doi:10.1073/pnas.1703553114

48. Rawlings ND, Barrett AJ. Families of cysteine peptidases. In: *Methods in Enzymology*. Vol 244. Proteolytic Enzymes: Serine and Cysteine Peptidases. Academic Press; 1994:461-486. doi:10.1016/0076-6879(94)44034-4

49. Liu W, Apagyi K, McLeavy L, Ersfeld K. Expression and cellular localisation of calpain-like proteins in *Trypanosoma brucei*. *Mol Biochem Parasitol*. 2010;169(1):20-26. doi:10.1016/j.molbiopara.2009.09.004

50. DaRocha WD, Silva RA, Bartholomeu DC, Pires SF, Freitas JM, Macedo AM, Vazquez MP, Levin MJ, Teixeira SMR. Expression of exogenous genes in *Trypanosoma cruzi*: improving vectors and electroporation protocols. *Parasitol Res*. 2004;92(2):113-120. doi:10.1007/s00436-003-1004-5

51. Dumoulin PC, Vollrath J, Won MM, Wang JX, Burleigh BA. Endogenous Sterol Synthesis Is Dispensable for *Trypanosoma cruzi* Epimastigote Growth but Not Stress Tolerance. *Front Microbiol*. 2022;13:937910. doi:10.3389/fmicb.2022.937910

52. Schumann Burkard G, Jutzi P, Roditi I. Genome-wide RNAi screens in bloodstream form trypanosomes identify drug transporters. *Mol Biochem Parasitol*. 2011;175(1):91-94. doi:10.1016/j.molbiopara.2010.09.002

53. Lander N, Chiurillo MA, Vercesi AE, Docampo R. Endogenous C-terminal Tagging by CRISPR/Cas9 in *Trypanosoma cruzi*. *Bio-Protoc*. 2017;7(10). doi:10.21769/BioProtoc.2299

54. Tarleton R, Peng D. EuPaGDT: a web tool tailored to design CRISPR guide RNAs for eukaryotic pathogens. *Microb Genomics*. 2015;1(4). doi:10.1099/mgen.0.000033

55. Kelly FD, Tran KD, Hatfield J, Schmidt K, Sanchez MA, Landfear SM. A Cytoskeletal Protein Complex is Essential for Division of Intracellular Amastigotes of *Leishmania mexicana*. *bioRxiv*. Published online April 30, 2020:2020.04.29.068445. doi:10.1101/2020.04.29.068445

56. Bangs JD, Uyetake L, Brickman MJ, Balber AE, Boothroyd JC. Molecular cloning and cellular localization of a BiP homologue in *Trypanosoma brucei*. Divergent ER retention signals in a lower eukaryote. *J Cell Sci*. 1993;105 (Pt 4):1101-1113.

57. Rappsilber J, Ishihama Y, Mann M. Stop and go extraction tips for matrix-assisted laser desorption/ionization, nanoelectrospray, and LC/MS sample pretreatment in proteomics. *Anal Chem*. 2003;75(3):663-670. doi:10.1021/ac026117i

58. Cox J, Mann M. MaxQuant enables high peptide identification rates, individualized p.p.b.-range mass accuracies and proteome-wide protein quantification. *Nat Biotechnol*. 2008;26(12):1367-1372. doi:10.1038/nbt.1511

59. Cox J, Neuhauser N, Michalski A, Scheltema RA, Olsen JV, Mann M. Andromeda: a peptide search engine integrated into the MaxQuant environment. *J Proteome Res*. 2011;10(4):1794-1805. doi:10.1021/pr101065j

60. Bruderer R, Bernhardt OM, Gandhi T, Reiter L. High-precision iRT prediction in the targeted analysis of data-independent acquisition and its impact on identification and quantitation. *Proteomics*. 2016;16(15-16):2246-2256. doi:10.1002/pmic.201500488

61. Bruderer R, Bernhardt OM, Gandhi T, Miladinović SM, Cheng LY, Messner S, Ehrenberger T, Zanotelli V, Butscheid Y, Escher C, Vitek O, Rinner O, Reiter L. Extending the limits of quantitative proteome profiling with data-independent acquisition and application to acetaminophen-treated three-dimensional liver microtissues. *Mol Cell Proteomics MCP*. 2015;14(5):1400-1410. doi:10.1074/mcp.M114.044305

62. Pang Z, Zhou G, Ewald J, Chang L, Hacariz O, Basu N, Xia J. Using MetaboAnalyst 5.0 for LC-HRMS spectra processing, multi-omics integration and covariate adjustment of global metabolomics data. *Nat Protoc*. 2022;17(8):1735-1761. doi:10.1038/s41596-022-00710-w

63. Sherman BT, Hao M, Qiu J, Jiao X, Baseler MW, Lane HC, Imamichi T, Chang W. DAVID: a web server for functional enrichment analysis and functional annotation of gene lists (2021 update). *Nucleic Acids Res*. Published online March 23, 2022:gkac194. doi:10.1093/nar/gkac194

64. Maric D, Olson CL, Xu X, Ames JB, Engman DM. Calcium-dependent membrane association of a flagellar calcium sensor does not require calcium binding. *Mol Biochem Parasitol*. 2015;201(1):72-75. doi:10.1016/j.molbiopara.2015.06.003

65. Schindelin J, Arganda-Carreras I, Frise E, Kaynig V, Longair M, Pietzsch T, Preibisch S, Rueden C, Saalfeld S, Schmid B, Tinevez JY, White DJ, Hartenstein V, Eliceiri K, Tomancak P, Cardona A. Fiji: an open-source platform for biological-image analysis. *Nat Methods*. 2012;9(7):676-682. doi:10.1038/nmeth.2019

Figure Legends

Figure 1. *T. cruzi* life cycle and schematic of TurboID-expressing lines generated for proximity-dependent biotinylation experiments. (**A**) Live confocal images of SMP1-1-GFP localized to the flagellum of *T. cruzi* epimastigotes and an intracellular amastigote; white oval denotes position of amastigote body. (**B**) Strategy for generating stable *T. cruzi* lines expressing TurboID in the flagellum using SMP1-1 as the

834 endogenous bait protein or in the cytoplasm of epimastigotes and amastigotes, where
835 addition of exogenous biotin will mediate biotinylation (red star) of proteins in close
836 proximity to TurboID in both settings. FLAG-epitope is included to facilitate TurboID
837 localization in transfectants. (**C**) Flow chart outlining the experimental protocol used for
838 identification of biotinylated proteins in epimastigotes (*left*) and intracellular amastigotes
839 (*right*). For both life stages, wild-type *('WT')*, cytoplasmic-TurboID ('*C'*) and flagellar-
840 TurboID ('*F'*) parasites (from left to right in the illustration) were exposed to biotin and
841 the biotinylated protein fraction in protein lysates captured on streptavidin-agarose
842 beads and subjected to mass spectrometry for identification and subsequent proteomic
843 analysis.
844
845 **Figure 2. TurboID localization and activity in *T. cruzi*.** (**A,C**) Fluorescence
846 microscopy images of fixed *T. cruzi* epimastigotes (**A**) or amastigotes (**C**) expressing
847 SMP1-1-FLAG-TurboID (F-Turbo) (*top*) or FLAG-TurboID (C-Turbo) (*bottom*) stained for
848 FLAG epitope (anti-FLAG)(*pink*). In (**C**), white arrows indicate the position of the
849 amastigote flagellum. (**B,D**) Biotinylated proteins in lysates of WT, F-Turbo, and C-
850 Turbo *T. cruzi* epimastigote (**B**) and amastigotes (**D**) detected with streptavidin-
851 Dylight800.
852
853 **Figure 3. Proximity proteome analysis identifies flagellar-enriched proteins in *T.***
854 ***cruzi*.** Principal component analysis (PCA) of biotinylome data plotted for WT (*no*
855 *TurboID control*), flagellar-TurboID (*F-Turbo*) and cytosolic-TurboID (*C-Turbo*) for *T.*
856 *cruzi* epimastigotes (**A**) and intracellular amastigotes (**C**). The two independent F-Turbo

857 groups in the epimastigote PCA plot are represented in green (triangles and squares).
858 Volcano plots (**B,D**) with fold-change (F-Turbo vs C-Turbo; x-axis) and adjusted p-value
859 (q-value; y-axis) for *T. cruzi* epimastigote (**B**) and amastigote (**D**) proteomic data.
860 Horizontal lines represent a q-value of 0.01 and the two vertical lines indicate the cut-
861 offs for fold change (2-fold). The top right quadrants in each plot (**B,D**) contain proteins
862 that are significantly enriched in F-Turbo proteomes ($q \leq 0.01$, $\geq$2-fold change). Known
863 trypanosomatid flagellar proteins (*purple circles)* and hypothetical proteins *(green*
864 *circles*) are shown for the F-Turbo enriched proteins. (**E**) Venn diagram depicting the
865 number of proteins identified as enriched in the F-Turbo samples of *T. cruzi*
866 epimastigote and amastigote stages. **(F**) Interpro domains assigned by DAVID that are
867 significantly enriched in F-Turbo samples (i.e. proteins found in the upper right quadrant
868 of each volcano plot) in epimastigotes, amastigotes and those common to both life
869 stages; *p*-value is a modified Fisher exact, for protein enrichment analysis.
870
871 **Figure 4. Flagellar localization of candidate flagellar proteins in *T. cruzi*.**
872 Endogenous tagging reveals flagellar localization of candidate flagellar proteins: calpain
873 1.3-smFLAG (TcCLB.506563.200), CARP3-smFLAG (TcCLB.506681.40), or
874 hypothetical protein-FLAG (TcCLB.510329.180) in *T. cruzi* epimastigotes (**A**) or
875 intracellular amastigotes (**B**)**.** In all cases, the FLAG tag was detected in fixed parasites
876 using an anti-FLAG antibody and secondary antibody (*green*) and the flagellum was
877 detected using anti-FCaBP and secondary antibody (*magenta*). The FLAG signal in the
878 flagellum is indicated (*yellow arrow*).
879

880 **Supplementary Figure 1. Model of the *T. cruzi* life cycle**. Schematic of the *T. cruzi*
881 life cycle highlighting the insect stage '*epimastigote*' that is propagated axenically in
882 liquid culture and gives rise to the infectious '*metacyclic trypomastigote*'.
883 Trypomastigotes, whether derived from epimastigotes or as the end product of a single
884 lytic cycle in a mammalian cell are motile, non-dividing forms of the parasite that actively
885 invade a mammalian host cell. Inside a host cell, the '*trypomastigote'* transforms into the
886 replicative intracellular '*amastigote'* stage by 18 hours post-infection (hpi). Amastigotes
887 undergo several rounds of proliferation, dividing by binary fission (between ~24-90 hpi),
888 before they stop dividing and differentiate into trypomastigotes, that eventually lyse the
889 infected host cell and disseminate infection. Stable transfection and drug selection is
890 performed in the epimastigote stage (lightning bolt symbolizes electroporation). Once
891 stable genomic changes are confirmed in epimastigotes, these parasites are used to
892 establish the mammalian infection cycle starting with metacyclic trypomastigotes as
893 outlined above.
894
895 **Supplementary Figure 2: PCR confirmation of endogenous tags for candidate**
896 **proteins. A.** Schematic showing the region of amplification and DNA gel with
897 corresponding bands for **A**. calpain 1.3-smFLAG (TcCLB.506563.200), **B.** CARP3-
898 smFLAG (TcCLB.506681.40), and **C.** hypothetical protein-FLAG (TcCLB.510329.180).
899 Ladder run on all DNA gels is Thermo Scientific GeneRuler DNA Ladder.
900

901 **Supplementary Table 1: Raw proteomics data for epimastigotes and intracellular**
902 **amastigotes TurboID experiment.** Each sheet contains the protein identity and
903 intensity score for all samples in either epimastigotes or amastigotes.
904
905 **Supplementary Table 2: Filtered proteomics data for epimastigotes and**
906 **intracellular amastigotes TurboID experiment.** Each sheet contains the protein
907 identity and intensity score for all samples in either epimastigotes or amastigotes that
908 was used for statistical analysis.
909
910 **Supplementary Table 3: Proteins enriched in the flagellar TurboID expressing**
911 **samples for epimastigotes and intracellular amastigotes**. Each sheet contains
912 information about the proteins enriched in either epimastigotes, amastigotes, or both
913 epimastigotes and amastigotes.
914
915 **Supplementary Table 4: Primers for all PCR and endogenous tagging**. Primer pairs
916 are listed for all experiments described.
917

Table 1: Candidate flagellar proteins in *T. cruzi* selected for endogenous tagging**.**

Name	TriTryp ID	Successfully Tagged?	Reason for selection
Calpain 1.3	TcCLB.506563.200	Yes	Potential signaling role
CARP3	TcCLB.506681.40	Yes	Potential signaling role
Hypothetical Protein	TcCLB.510329.180	Yes	No known ortholog
Hypothetical Protein	TcCLB.509965.20	Yes	No known *T. brucei* ortholog
ATPase	TcCLB.506925.410	No	Potential transmembrane protein
Hypothetical Protein	TcCLB.509011.50	No	Potential signaling role

Candidates from the 40 proteins identified in both *T. cruzi* epimastigotes and amastigotes selected for endogenous epitope tagging and localization.

Figure 1: Won et al.

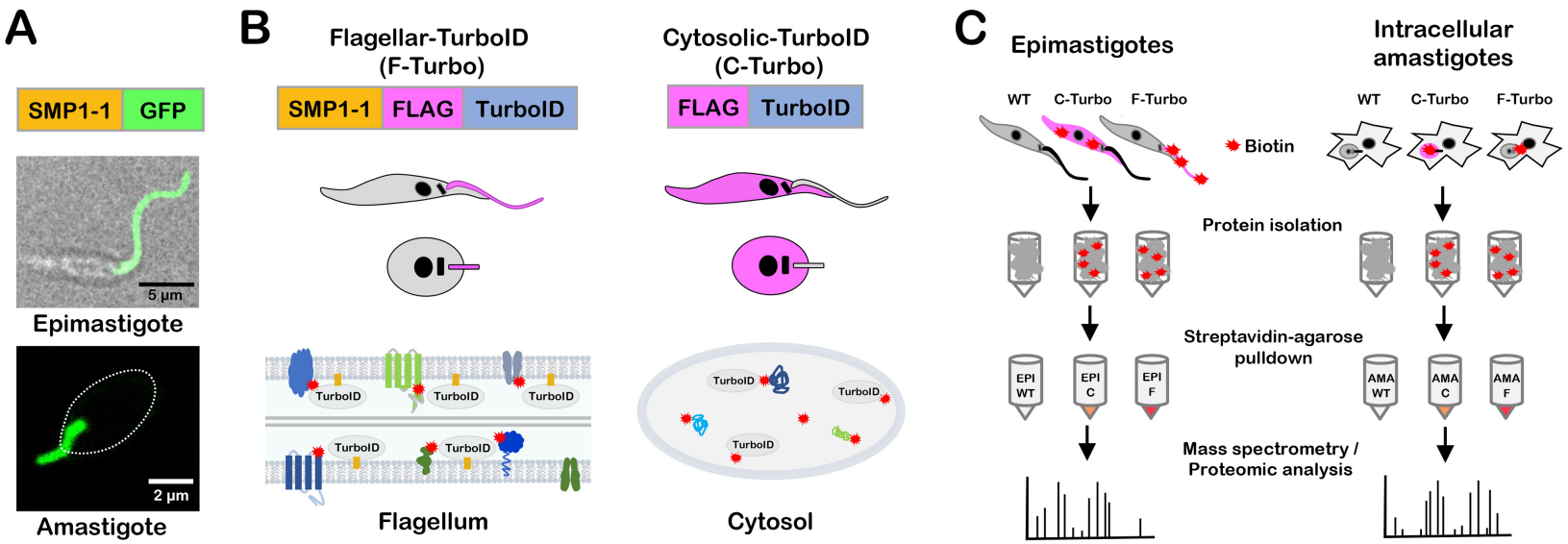

Figure 1. *T. cruzi* life cycle and schematic of TurboID-expressing lines generated for proximity-dependent biotinylation experiments. (**A**) Live confocal images of SMP1-1-GFP localized to the flagellum of *T. cruzi* epimastigotes and an intracellular amastigote; white oval denotes position of amastigote body. (**B**) Strategy for generating stable *T. cruzi* lines expressing TurboID in the flagellum using SMP1-1 as the endogenous bait protein or in the cytoplasm of epimastigotes and amastigotes, where addition of exogenous biotin will mediate biotinylation (red star) of proteins in close proximity to TurboID in both settings. FLAG-epitope is included to facilitate TurboID localization in transfectants. (**C**) Flow chart outlining the experimental protocol used for identification of biotinylated proteins in epimastigotes (*left*) and intracellular amastigotes (*right*). For both life stages, wild-type (*'WT'*), cytoplasmic-TurboID ('*C*') and flagellar-TurboID ('*F*') parasites (from left to right in the illustration) were exposed to biotin and the biotinylated protein fraction in protein lysates captured on streptavidin-agarose beads and subjected to mass spectrometry for identification and subsequent proteomic analysis.

Figure 2: Won et al.

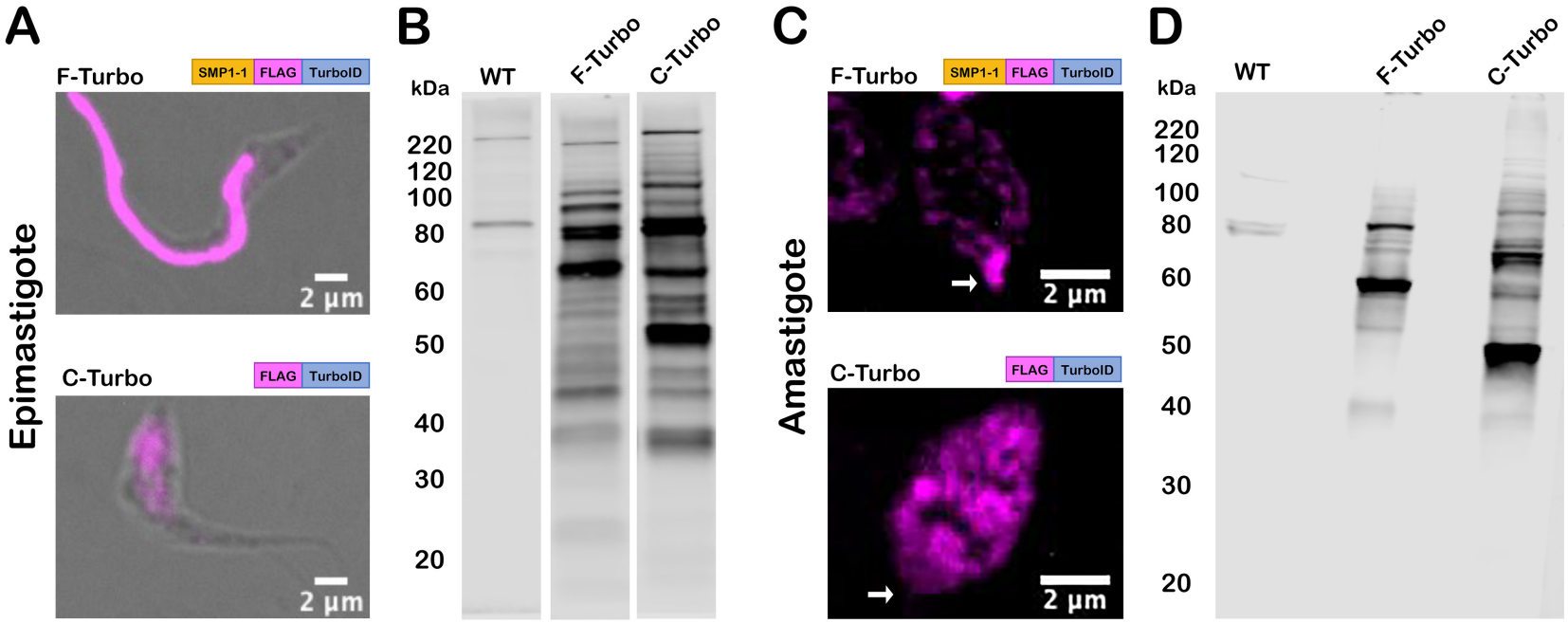

Figure 2. TurboID localization and activity in *T. cruzi*. (**A**,**C**) Fluorescence microscopy images of fixed *T. cruzi* epimastigotes (**A**) or amastigotes (**C**) expressing SMP1-1-FLAG-TurboID (F-Turbo) (*top*) or FLAG-TurboID (C-Turbo) (*bottom*) stained for FLAG epitope (anti-FLAG)(*pink*). In (**C**), white arrows indicate the position of the amastigote flagellum. (**B**,**D**) Biotinylated proteins in lysates of WT, F-Turbo, and C-Turbo *T. cruzi* epimastigote (**B**) and amastigotes (**D**) detected with streptavidin-Dylight800.

Figure 3: Won et al.

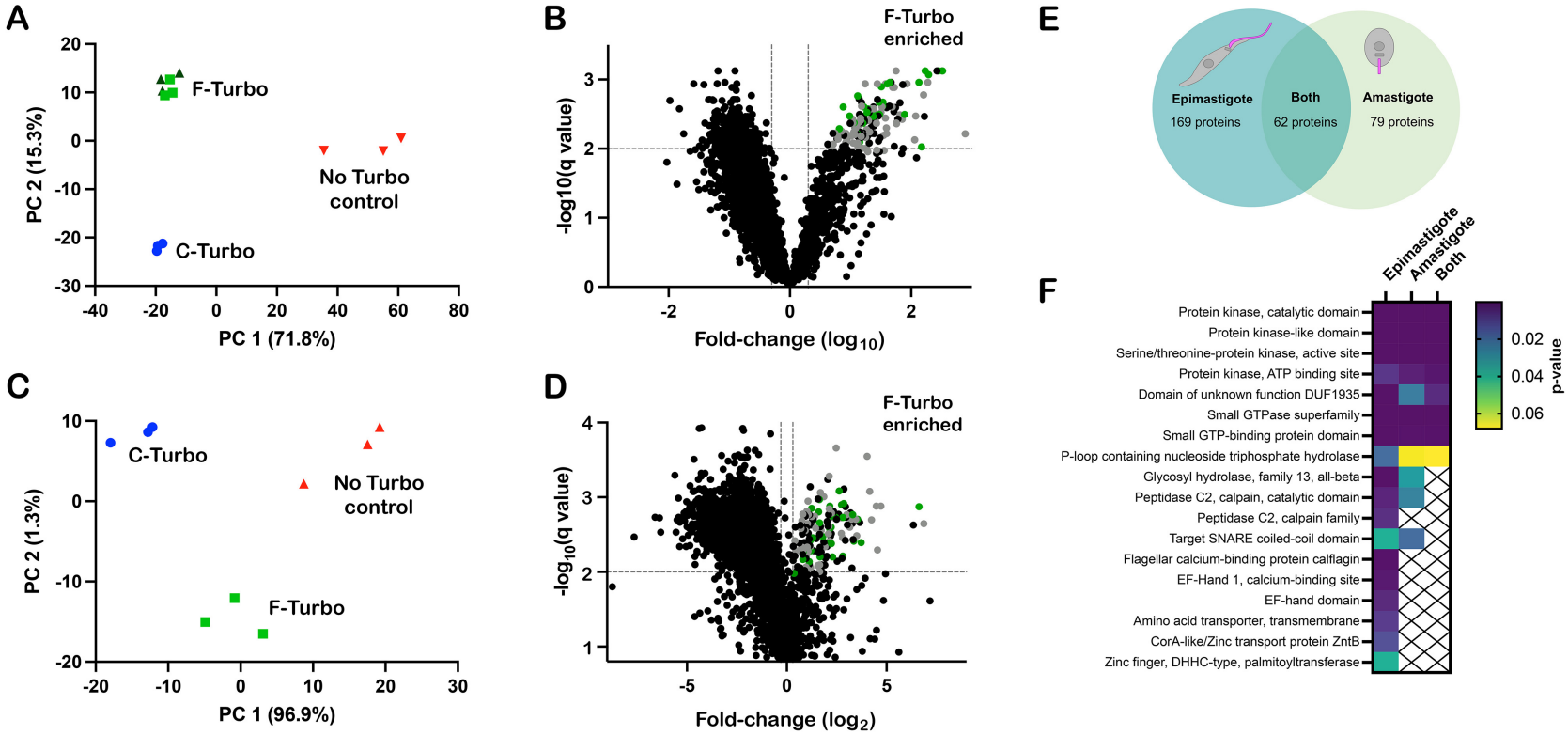

Figure 3. Proximity proteome analysis identifies flagellar-enriched proteins in *T. cruzi*. Principal component analysis (PCA) of biotinylome data plotted for WT (*no TurboID control*), flagellar-TurboID (*F-Turbo*) and cytosolic-TurboID (*C-Turbo*) for *T. cruzi* epimastigotes (**A**) and intracellular amastigotes (**C**). The two independent F-Turbo groups in the epimastigote PCA plot are represented in green (triangles and squares). Volcano plots (**B,D**) with fold-change (F-Turbo vs C-Turbo; x-axis) and adjusted p-value (q-value; y-axis) for *T. cruzi* epimastigote (**B**) and amastigote (**D**) proteomic data. Horizontal lines represent a q-value of 0.01 and the two vertical lines indicate the cut-offs for fold change (2-fold). The top right quadrants in each plot (**B,D**) contain proteins that are significantly enriched in F-Turbo proteomes ($q \leq 0.01$, $\geq$2-fold change). Known trypanosomatid flagellar proteins (*purple circles)* and hypothetical proteins *(green circles*) are shown for the F-Turbo enriched proteins. (**E**) Venn diagram depicting the number of proteins identified as enriched in the F-Turbo samples of *T. cruzi* epimastigote and amastigote stages. **(F**) Interpro domains assigned by DAVID that are significantly enriched in F-Turbo samples (i.e. proteins found in the upper right quadrant of each volcano plot) in epimastigotes, amastigotes and those common to both life stages; *p*-value is a modified Fisher exact, for protein enrichment analysis.

Figure 4: Won et al.

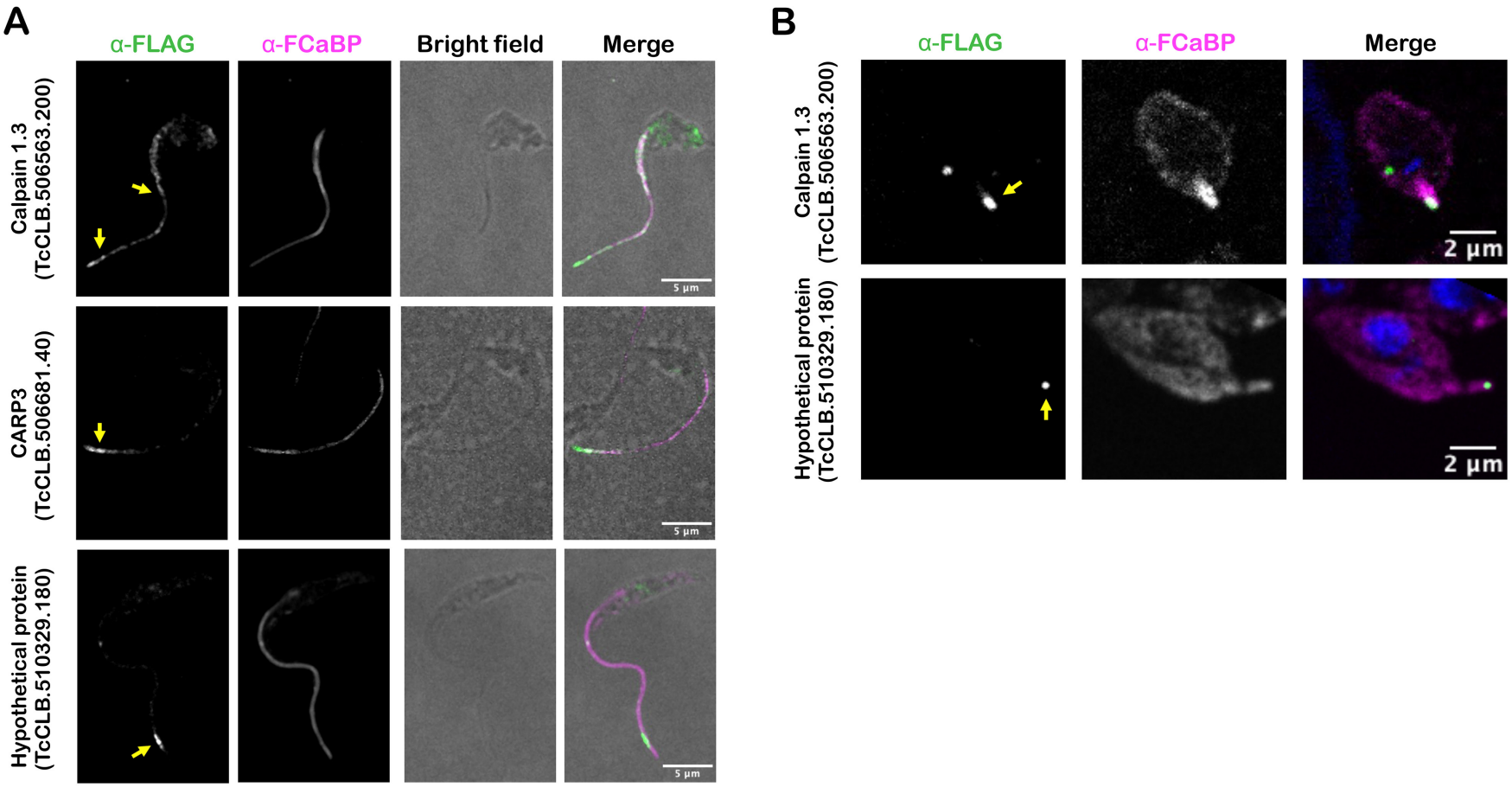

Figure 4. Flagellar localization of candidate flagellar proteins in *T. cruzi*. Endogenous tagging reveals flagellar localization of candidate flagellar proteins: calpain 1.3-smFLAG (TcCLB.506563.200), CARP3-smFLAG (TcCLB.506681.40), or hypothetical protein-FLAG (TcCLB.510329.180) in *T. cruzi* epimastigotes (**A**) or intracellular amastigotes (**B**). In all cases, the FLAG tag was detected in fixed parasites using an anti-FLAG antibody and secondary antibody (*green*) and the flagellum was detected using anti-FCaBP and secondary antibody (*magenta*). The FLAG signal in the flagellum is indicated (*yellow arrow*).

Supplemental Figure 1: Won et al.

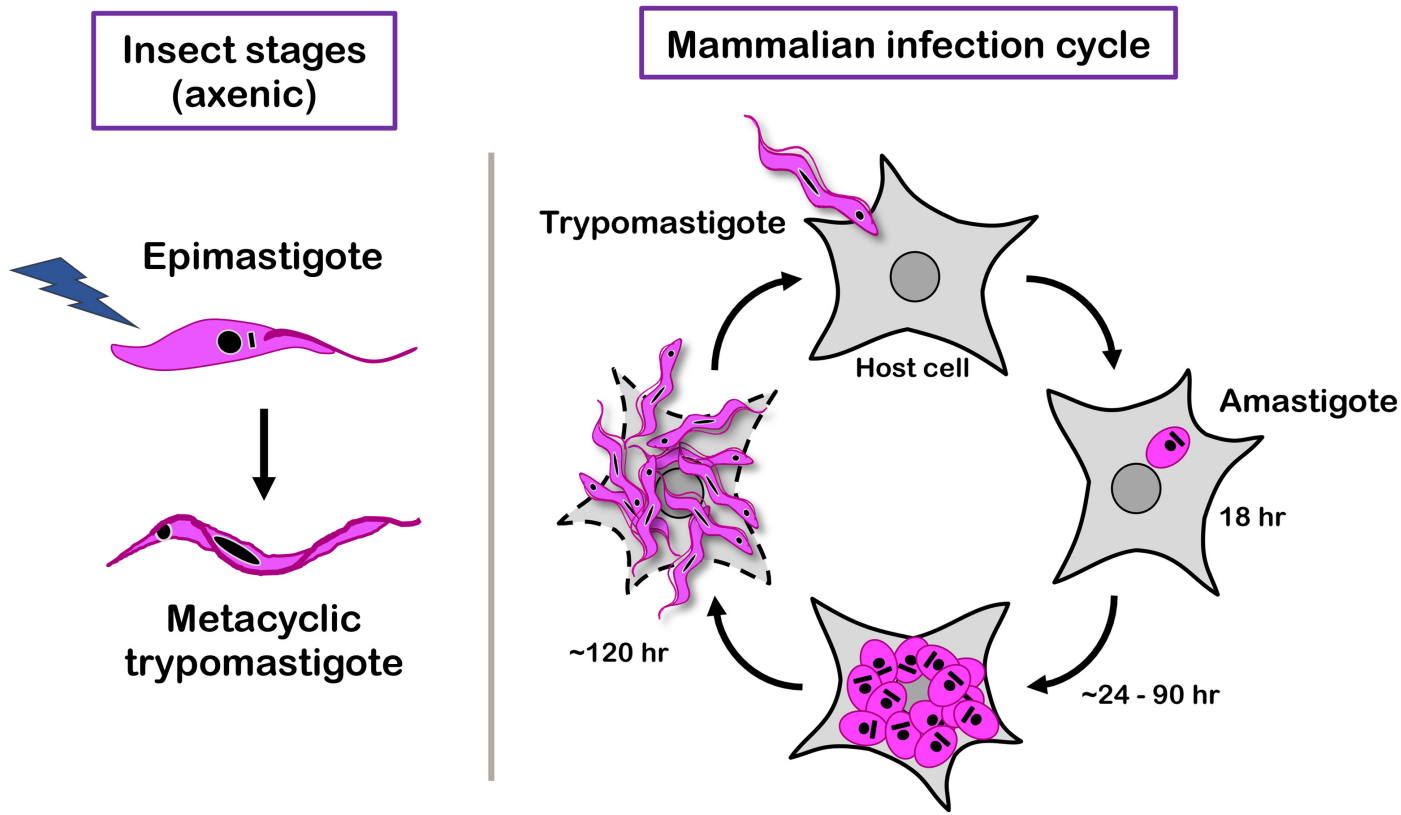

Supplemental Figure 1. **Schematic of the *T. cruzi* life cycle**. Insect stage '*epimastigote*' that is propagated axenically in liquid culture and gives rise to the infectious '*metacyclic trypomastigote*'. Trypomastigotes, whether derived from epimastigotes or as the end product of a single lytic cycle in a mammalian cell are motile, non-dividing forms of the parasite that actively invade a mammalian host cell. Inside a host cell, the '*trypomastigote'* transforms into the replicative intracellular '*amastigote'* stage by 18 hours post-infection (hpi). Amastigotes undergo several rounds of proliferation, dividing by binary fission (between ~24-90 hpi), before they stop dividing and differentiate into trypomastigotes, that eventually lyepimastigotese the infected host cell and disseminate infection. Stable transfection and drug selection is performed in the stage (lightning bolt symbolizes electroporation). Once stable genomic changes are confirmed in epimastigotes, these parasites are used to establish the mammalian infection cycle starting with metacyclic trypomastigotes as outlined above.

Supplemental Figure 2: Won et al.

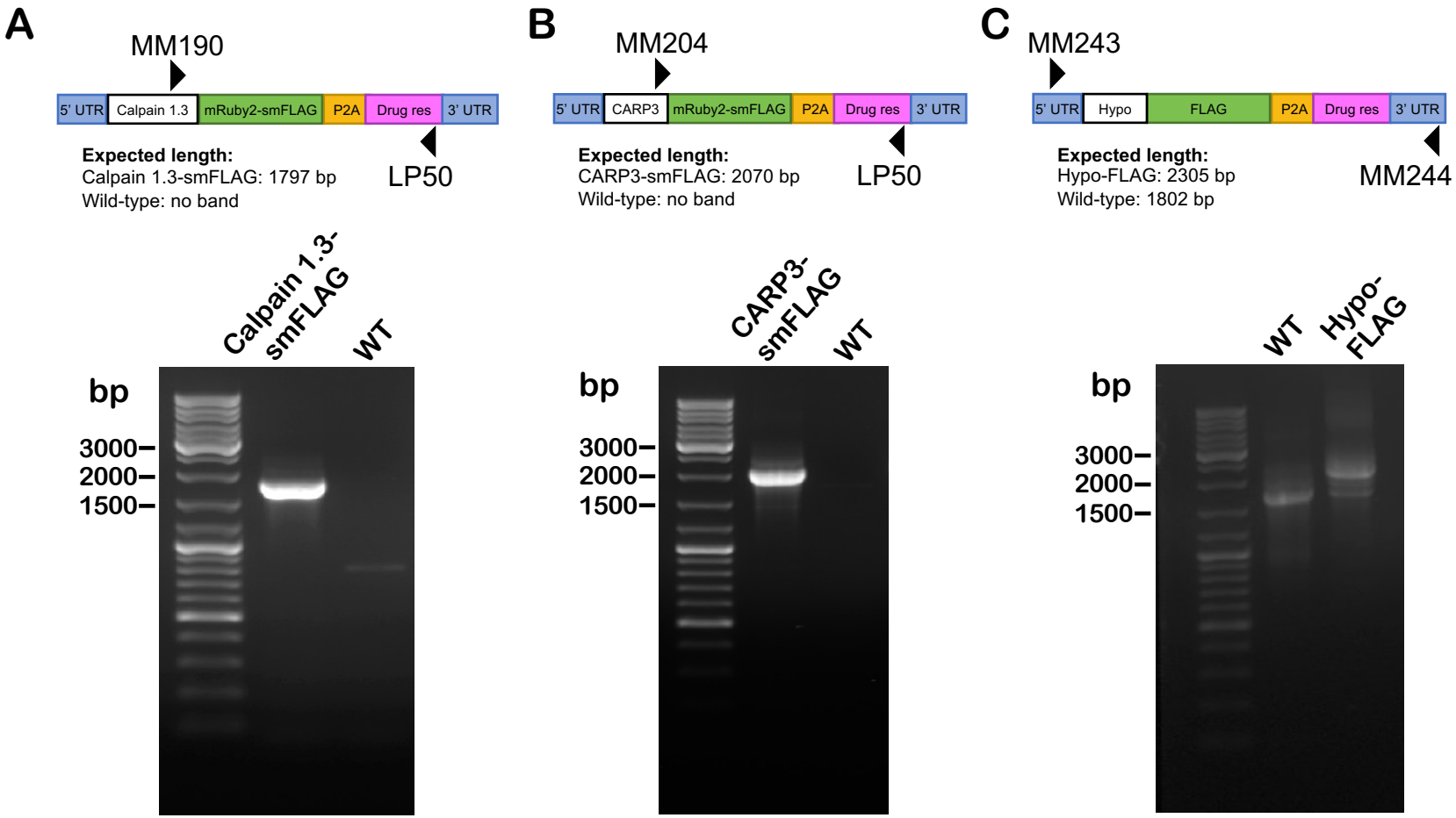

Supplemental Figure 2: PCR confirmation of endogenous tags for candidate proteins. A. Schematic showing the region of amplification and DNA gel with corresponding bands for **A**. calpain 1.3-smFLAG (TcCLB.506563.200), **B.** CARP3-smFLAG (TcCLB.506681.40), and **C.** hypothetical protein-FLAG (TcCLB.510329.180). DNA ladder shown with sizes (bp) on left.